INTERNATIONAL JOURNAL FOR NUMERICAL METHODS IN FLUIDS
Int. J. Numer. Meth. Fluids 2001; **35**: 371–394

Applications of a higher-order bounded numerical scheme to turbulent flows

B. Song[a], G. R. Liu[a] and R. S. Amano[b,*,1]

[a] *Institute of High Performance Computing, The Rutherford Singapore Science Park 1, Singapore, Singapore*
[b] *Department of Mechanical Engineering, University of Wisconsin-Milwaukee, Milwaukee, WI, U.S.A.*

SUMMARY

This paper applies the higher-order bounded numerical scheme Weighted Average Coefficients Ensuring Boundedness (WACEB) to simulate two- and three-dimensional turbulent flows. In the scheme, a weighted average formulation is used for interpolating the variables at cell faces and the weighted average coefficients are determined from a normalized variable formulation and total variation diminishing (TVD) constraints to ensure the boundedness of the solution. The scheme is applied to two turbulent flow problems: (1) two-dimensional turbulent flow around a blunt plate; and (2) three-dimensional turbulent flow inside a mildly curved U-bend. In the present study, turbulence is evaluated by using a low-Reynolds number version of the k–ω model. For the flow simulation, the QUICK scheme is applied to the momentum equations while either the WACEB scheme (Method 1) or the UPWIND scheme (Method 2) is used for the turbulence equations. The present study shows that the WACEB scheme has at least second-order accuracy while ensuring boundedness of the solutions. The present numerical study for a pure convection problem shows that the 'TVD' slope ranges from 2 to 4. For the turbulent recirculating flow, two different mixed procedures (Method 1 and Method 2) produce a substantial difference for the mean velocities as well as for the turbulence kinetic energy. Method 1 predicts better results than Method 2 does, comparing the analytical solution and the experimental data. For the turbulent flow inside the mildly curved U-bend, although the predictions of velocity distributions with two procedures are very close, a noticeable difference of turbulence kinetic energy is exhibited. It is noticed that the discrepancy exists between numerical results and the experimental data. The reason is the limit of the two-equation turbulence model to such complex turbulent flows with extra strain-rates. Copyright © 2001 John Wiley & Sons, Ltd.

KEY WORDS: bounded numerical scheme; turbulent flow; turbulence model

* Correspondence to: Department of Mechanical Engineering, College of Engineering and Applied Science, University of Wisconsin-Milwaukee, PO Box 784, Milwaukee, WI 53201, U.S.A.
[1] E-mail: amano@uwm.edu

Received 18 October 1999
Revised 22 March 2000

1. INTRODUCTION

Numerical studies of turbulent flows in engineering demand, apart from mathematical representations of the turbulent motion, a general, flexible, efficient, accurate, and—perhaps most importantly—stable and bounded numerical algorithms for the solution of a complete set of average equations and turbulence equations. Formulation of the approximation scheme for convection fluxes may be one of the major tasks to meet such demands.

The classical first-order schemes, such as UPWIND, HYBRID, and POWER-LAW, are unconditionally bounded but tend to misrepresent the transport processes through the accumulation of a numerical diffusion rate arising from flow-to-grid skewness. Higher-order schemes, such as second-order upwind [1], third-order upwind (QUICK) [2], four-point third-order interpolation (FPTOI), and four-point fourth-order interpolation (FPFOI) [3] schemes, offer a route to improving the accuracy of computations. However, all suffer from a lack of the boundedness problem, i.e., their solutions may display overshoots and undershoots. In some applications, small overshoots and undershoots may be tolerable. However, under some circumstances, the non-linear processes of turbulence will feed back and amplify these overshoots and undershoots and may lead to the divergence of a solution. The conventional method for simulating turbulent flows is that the QUICK scheme is used for the momentum equations and the UPWIND or HYBRID scheme is used for turbulence equations, such as the turbulence kinetic energy equation, the dissipation rate equation, and the Reynolds stress equations. However, we should be always suspicious of the first-order schemes since they have poor track records.

In the last decade, efforts have been made to derive high resolution and bounded schemes. Zhu and Leschnizer [4] proposed a local oscillation-damping algorithm (LODA). Since the LODA scheme introduces contributions from the UPWIND scheme, second-order diffusion is introduced into those regions where QUICK displays unbounded behavior. In 1988, Leonard [5] developed a normalized variable formulation and presented a high resolution bounded scheme called Simple High-Accuracy Resolution Program (SHARP). Gaskell and Lau [6] developed a scheme called Sharp And Monotonic Algorithm for Realistic Transport (SMART) by using a curvature compensated convective transport approximation and a piecewise linear normalized variable formulation. However, numerical testing [7] shows that both SMART and SHARP need an under-relaxation treatment at each of the control volume cell faces in order to overcome the oscillation behavior. This drawback leads to an increase in the computer storage requirement, especially for three-dimensional flow calculations. Song *et al.* [8] proposed a higher-order scheme called Weighted Average Coefficients Ensuring Boundedness (WACEB). Combining Taylor expansion and total variation diminishing (TVD) constraints, they used a weighted average formulation to interpolate the variables at cell faces and then to construct the WACEB scheme. Their numerical tests on laminar flow fields with steep gradients showed that the WACEB scheme has at least second-order accuracy while ensuring boundedness of the solution and is easily implemented in a general computer program.

In the present study, we aim to extend the WACEB scheme to simulate turbulent flows. Turbulence is represented by a low-Reynolds number version of the $k-\omega$ model [9]. Two flow problems are simulated: (1) two-dimensional turbulent flow around a blunt plate; and (2) three-dimensional turbulent flow inside a moderate curved U-bend. For flow simulation, two

mixed procedures of numerical schemes are employed. One is a traditional way in which the QUICK scheme is used for the momentum equations and the UPWIND scheme is applied for the turbulence equations (Method 2). The another is a new approach in which QUICK is used for the momentum equations and WACEB is applied for the turbulence equations. The choice of 'TVD' slope will be numerically studied. Furthermore, the predicted results are compared with experimental data.

2. GOVERNING EQUATIONS AND WACEB SCHEME

2.1. Governing equations and their discretization

The averaged governing equations for incompressible Reynolds averaged turbulent flows can be written in general tensorial form

$$\frac{\partial u_i \Phi}{\partial x_i} = \frac{\partial}{\partial x_i}\left(\Gamma^{\Phi}\frac{\partial \Phi}{\partial x_i}\right) + S_{\Phi} \tag{1}$$

where the diffusive coefficient Γ^{Φ} and the source term S_{Φ} in the Cartesian co-ordinate system are given in Table I for different dependent variables Φ.

Here, a low-Reynolds number version of the k–ω model [9] is used to represent turbulence. The constants in the model are given in Table II.

With ξ, η, ζ representing a general curvilinear co-ordinate system in a three-dimensional framework, Equation (1) can be expressed as

Table I. Form of terms in the individual equations.

Φ	Γ^{Φ}	S_{Φ}
1	1	0
u	$v+v_t$	$-\frac{1}{\rho}\frac{\partial P}{\partial x}+\frac{\partial}{\partial x}\left(\Gamma^{\Phi}\frac{\partial u}{\partial x}\right)+\frac{\partial}{\partial y}\left(\Gamma^{\Phi}\frac{\partial v}{\partial x}\right)+\frac{\partial}{\partial z}\left(\Gamma^{\Phi}\frac{\partial w}{\partial x}\right)$
v	$v+v_t$	$-\frac{1}{\rho}\frac{\partial P}{\partial y}+\frac{\partial}{\partial x}\left(\Gamma^{\Phi}\frac{\partial u}{\partial y}\right)+\frac{\partial}{\partial y}\left(\Gamma^{\Phi}\frac{\partial v}{\partial y}\right)+\frac{\partial}{\partial z}\left(\Gamma^{\Phi}\frac{\partial w}{\partial y}\right)$
w	$v+v_t$	$-\frac{1}{\rho}\frac{\partial P}{\partial z}+\frac{\partial}{\partial x}\left(\Gamma^{\Phi}\frac{\partial u}{\partial z}\right)+\frac{\partial}{\partial y}\left(\Gamma^{\Phi}\frac{\partial v}{\partial z}\right)+\frac{\partial}{\partial z}\left(\Gamma^{\Phi}\frac{\partial w}{\partial z}\right)$
k	$v+\sigma^* v_t$	$P_k-\beta^*\omega k$
ω	$v+\sigma v_t$	$\alpha\frac{\omega}{k}P_k-\beta\omega^2$

$$\alpha^* = \frac{\alpha_0^* + Re_T/R_k}{1+Re_T/R_k}, \quad \alpha = \frac{5}{9}\frac{\alpha_0+Re_T/R_\omega}{1+Re_T/R_\omega}(\alpha^*)^{-1}, \quad \beta^* = \frac{9}{100}\frac{5/18+(Re_T/R_\beta)^4}{1+(Re_T/R_\beta)^4}$$

$$Re_T = \frac{k}{\omega v}, \quad P_k = \text{turbulence energy production rate}$$

Table II. Constants.

$\sigma = \sigma^*$	β	α_0^*	α_0	R_β	R_k	R_ω
0.5	3/40	1/40	1/10	8	6	27/10

$$\frac{1}{J}\left[\frac{\partial U\Phi}{\partial\xi}+\frac{\partial V\Phi}{\partial\eta}+\frac{\partial W\Phi}{\partial\zeta}\right]$$
$$=\frac{1}{J}\frac{\partial}{\partial\xi}\left[\frac{\Gamma_\Phi}{J}(q_{11}\Phi_\xi)\right]+\frac{1}{J}\frac{\partial}{\partial\eta}\left[\frac{\Gamma_\Phi}{J}(q_{22}\Phi_\eta)\right]+\frac{1}{J}\frac{\partial}{\partial\zeta}\left[\frac{\Gamma_\Phi}{J}(q_{33}\Phi_\zeta)\right]+S_\Phi^{\mathrm{CD}}+S_\Phi(\xi,\eta,\zeta) \tag{2}$$

where U, V, and W are contravariant velocities. They are defined as

$$U=j_{11}u+j_{21}v+j_{31}w$$

$$V=j_{12}u+j_{22}v+j_{32}w$$

$$W=j_{13}u+j_{23}v+j_{33}w$$

where J denotes the Jacobian, q_{ij} and j_{ij} are the transformation coefficients, and S_Φ^{CD} is the cross-diffusion term.

Following the control volume method for a non-staggered grid arrangement, Equation (2) can be discretized into an algebraic equation

$$A_P\Phi_P=\sum_{i=\mathrm{E,\,W,\,N,\,S,\,T,\,B}}A_i\Phi_i+b \tag{3}$$

where Φ_P represents the variable at a node P and the Φ_i are neighboring variables. In the discretization, the central differencing is used for the diffusion terms and the upwind differencing QUICK or higher-order bounded WACEB is used for the convection terms.

2.2. The higher-order bounded WACEB scheme

Consider the variation of a convected scalar Φ along a direction normal to a control volume cell face, as shown in Figure 1. For non-uniformly distributed grids, the scalar Φ at the cell face $(i-\frac{1}{2})$ can be determined from the bias-upwind weight average method, i.e.

$$\Phi_{i-1/2}=a\Phi_i+b\Phi_{i-1}+c\Phi_{i-2} \tag{4}$$

where a, b, and c are the weighted average coefficients, which satisfy the following relation:

$$a+b+c=1$$

Thus, Equation (4) can be rewritten as

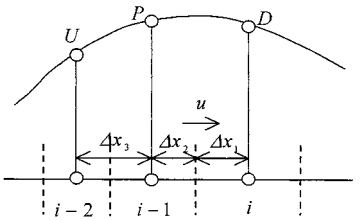

Figure 1. One-dimensional stencil and grid nodes.

$$\Phi_{i-1/2} = \underline{\Phi_{i-1}} + a(\Phi_i - \Phi_{i-1}) - c(\Phi_{i-1} - \Phi_{i-2}) \tag{5}$$

where the underlined term represents the fragment of the first-order UPWIND scheme.

Performing Taylor series expansions about the left and right nodes directly adjacent to call face $i-\frac{1}{2}$ gives

$$\Phi_i = \Phi_{i-1/2} + \Delta x_1 \Phi' + \frac{\Delta x_1^2}{2}\Phi'' + O(\Delta x_1^3) \tag{6a}$$

$$\Phi_{i-1} = \Phi_{i-1/2} - \Delta x_2 \Phi' + \frac{\Delta x_2^2}{2}\Phi'' + O(\Delta x_2^3) \tag{6b}$$

$$\Phi_{i-2} = \Phi_{i-1/2} - (\Delta x_2 + \Delta x_3)\Phi' + \frac{(\Delta x_2 + \Delta x_3)^2}{2}\Phi'' + O(\Delta x_3^3) \tag{6c}$$

Substitution of Equations (6) into Equation (5) yields

$$\begin{aligned}\Phi_{i-1/2} = \Phi_{i-1} + a(\Phi_i - \Phi_{i-1}) - c(\Phi_{i-1} - \Phi_{i-2}) + [-\Delta x_2 + a(\Delta x_1 + \Delta x_2) - c\Delta x_3]\Phi' \\ + \frac{1}{2}[\Delta x_2^2 + a(\Delta x_1 - \Delta x_2)(\Delta x_1 + \Delta x_2) + c\Delta x_3(2\Delta x_2 + \Delta x_3)]\Phi'' + O(\Delta x^3)\end{aligned} \tag{7}$$

Different order schemes can be achieved through the choices of the weight average coefficients a and c. For example, the third-order QUICK scheme can be obtained when the fourth and fifth terms become zero. That is

$$(\Delta x_1 + \Delta x_2)a - \Delta x_3 c = \Delta x_2 \tag{8a}$$

$$(\Delta x_1 + \Delta x_2)(\Delta x_1 - \Delta x_2)a + \Delta x_3(2\Delta x_2 + \Delta x_3)c = -\Delta x_2^2 \tag{8b}$$

Solving the above equations yields

$$a^{Q} = \frac{\Delta x_2(\Delta x_2 + \Delta x_3)}{(\Delta x_1 + \Delta x_2) \times (\Delta x_1 + \Delta x_2 + \Delta x_3)} \tag{9a}$$

$$c^{Q} = -\frac{\Delta x_1 \Delta x_2}{\Delta x_3(\Delta x_1 + \Delta x_2 + \Delta x_3)} \tag{9b}$$

where a^{Q} and c^{Q} are the weighted average coefficients for the QUICK scheme.

Based on the variable normalization proposed by Leonard [5], with a three-node stencil shown in Figure 1, we introduce a normalized variable defined as

$$\tilde{\Phi} = \frac{\Phi - \Phi_{\mathrm{U}}}{\Phi_{\mathrm{D}} - \Phi_{\mathrm{U}}}$$

where the subscripts U and D represent the upstream and the downstream locations. With the above definition, the weight average interpolation formulation (5) is rewritten in the following normalized form:

$$\tilde{\Phi}_{i-1/2} = a + (1 - a - c)\tilde{\Phi}_{i-1} \tag{10}$$

In order to ensure the boundedness of solutions, the scheme is required to satisfy the standard TVD constraints, i.e.

$$\begin{array}{ll} \tilde{\Phi}_{i-1/2} \le 1, \quad \tilde{\Phi}_{i-1/2} \le 2\Phi_{i-1}, \quad \tilde{\Phi}_{i-1/2} \ge \tilde{\Phi}_{i-1} & \text{for } 0 < \tilde{\Phi}_{i-1} < 1 \\ \tilde{\Phi}_{i-1/2} = \tilde{\Phi}_{i-1} & \text{for } \tilde{\Phi}_{i-1} \le 0 \quad \text{or} \quad \tilde{\Phi}_{i-1} \ge 1 \end{array} \tag{11}$$

which is corresponding to the triangle region shown in Figure 2. However, the standard TVD slope of 2 may be conversative and may add unnecessary artificial diffusion. Thus, the slope of C_s is used to replace 2.

From Equation (7) it is noted that the scheme has at least second-order accuracy as long as Equation (8a) is satisfied. Also, the maximum accuracy (third-order) can be achieved if the weight average coefficients are chosen based on Equation (9). Thus, the scheme can be formed in such a way that the weight average coefficient lies as close as possible to the values calculated in terms of Equation (9), while satisfying the TVD constraints to ensure the boundedness.

Combining Equations (8a) and (10), we can have

$$a = \frac{\Delta x_3 \tilde{\Phi}_{i-1/2} - (\Delta x_2 + \Delta x_3)\tilde{\Phi}_{i-1}}{\Delta x_3 - (\Delta x_1 + \Delta x_2 + \Delta x_3)\tilde{\Phi}_{i-1}} \tag{12a}$$

$$c = \frac{(\Delta x_1 + \Delta x_2)\tilde{\Phi}_{i-1/2} - \Delta x_1 \tilde{\Phi}_{i-1} - \Delta x_2}{\Delta x_3 - (\Delta x_1 + \Delta x_2 + \Delta x_3)\tilde{\Phi}_{i-1}} \tag{12b}$$

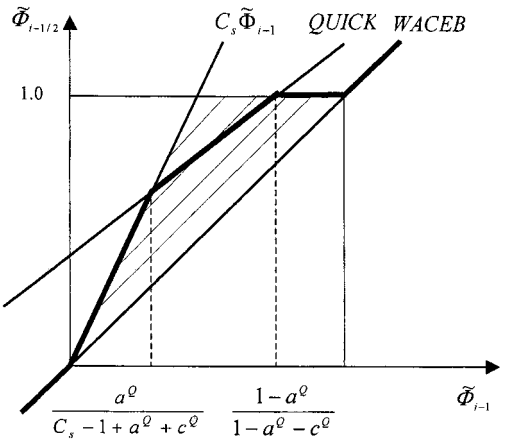

Figure 2. Normalized variable diagram for WACEB scheme.

Based on the above idea, the WACEB scheme can be constructed in the following way:

$$a^W,\ c^W = \begin{cases} a^Q,\ c^Q \text{ from Equation (9), if } \tilde{\Phi}_{i-1}\in[d_1, d_2] \\ a,\ c \text{ from Equation (12), if } \tilde{\Phi}_{i-1}\notin[d_1, d_2] \end{cases} \tag{13}$$

where d_1 and d_2 are calculated through

$$d_1 = \frac{a^Q}{C_s - 1 + a^Q + c^Q}$$

$$d_2 = \frac{1 - a^Q}{1 - a^Q - c^Q}$$

In Equation (12), the variable at cell face can be calculated through

$$\tilde{\Phi}_{i-1/2} = \begin{cases} C_s\tilde{\Phi}_{i-1} & \tilde{\Phi}_{i-1}\in[0, d_1) \\ a^Q + (1 - a^Q - c^Q)\tilde{\Phi}_{i-1} & \tilde{\Phi}_{i-1}\in[d_1, d_2] \\ 1 & \tilde{\Phi}_{i-1}\in(d_2, 1] \\ \tilde{\Phi}_{i-1} & \tilde{\Phi}_{i-1}\notin[0, 1] \end{cases} \tag{14}$$

where C_s is the TVD slope (see Figure 2). For standard TVD constraints, C_s is equal to 2.

It is noted that the underlined term in Equation (5) represents the fragment of the first-order upwind scheme. Therefore, the higher-order schemes, such as QUICK and WACEB, can be implemented in a deferred correction approach, as proposed by Khosla and Rubin [10]. That is

$$\Phi_f^{n+1} = \Phi_f^{\mathrm{UP},\,n+1} + (\Phi_f^{\mathrm{HO},\,n} - \Phi_f^{\mathrm{UP},\,n}) \tag{15}$$

where n indicates the iteration level, and UP and HO refer to the upwind and higher-order schemes respectively. The convective fluxes calculated by the upwind scheme are combined with the diffusion term to form the main coefficients of the difference equation, while those resulting from the deferred correction terms S_Φ^{DC} are collected into the source term in Equation (3). Such a treatment leads to an always diagonally dominant coefficient matrix and enables the higher-order accuracy to be achieved at the converged stage.

With this approach, the deferred correction source term, taking the east–west direction as an example, is calculated by

$$\begin{aligned} S_\Phi^{\mathrm{DC}} = {} & U_{\mathrm{e}}^{+} U_{\mathrm{e}}[a^W \Delta_{\mathrm{e}} - c^W \Delta_{\mathrm{e}}^{-}] - U_{\mathrm{e}}^{-} U_{\mathrm{e}}[a^W \Delta_{\mathrm{e}} - c^W \Delta_{\mathrm{e}}^{+}] - U_{\mathrm{w}}^{+} U_{\mathrm{w}}[a^W \Delta_{\mathrm{w}} - c^W \Delta_{\mathrm{w}}^{-}] \\ & + U_{\mathrm{w}}^{-} U_{\mathrm{w}}[a^W \Delta_{\mathrm{w}} - c^W \Delta_{\mathrm{w}}^{+}] \end{aligned} \tag{16}$$

where

$$\Delta_{\mathrm{e}}^{-} = \Phi_P - \Phi_{\mathrm{W}}, \qquad \Delta_{\mathrm{e}} = \Phi_{\mathrm{E}} - \Phi_P, \qquad \Delta_{\mathrm{e}}^{+} = \Phi_{\mathrm{EE}} - \Phi_{\mathrm{E}}$$

and

$$U_f^{\pm} = \frac{1 \pm \mathrm{sgn}(U_f)}{2}$$

The subscripts 'e' and 'w' represent the cell faces $i+\frac{1}{2}$ and $i-\frac{1}{2}$ respectively.

2.3. Mixed procedures of numerical schemes

Theoretically, the third-order QUICK scheme can be used to achieve very accurate numerical results. However, it often suffers from a lack of boundedness; i.e., the solution may display overshoots and undershoots. When applying it to solve turbulence transport equations, the non-linear processes of turbulent diffusion will feed back and may amplify these overshoots and undershoots, thus leading to numerical instability.

In order to overcome the boundedness problem of QUICK, the traditional way of simulating turbulent flows is that the QUICK scheme is applied to the momentum equations and the UPWIND scheme is used for turbulence equations, which is called Method 2 here. In the present study, a different mixed procedure, which is called Method 1, is used. The QUICK scheme is applied to the momentum equations and the WACEB scheme is used for turbulence equations.

It is necessary to mention that the QUICK and WACEB schemes all need two upstream nodes for each cell face, which will involve a value outside the solution domain for a

near-boundary control volume. Therefore, the UPWIND scheme is used for all control volumes that are adjacent to boundaries.

2.4. Numerical solution procedure

The calculation presented in this paper was carried out with a general-purpose computer code designed to solve incompressible elliptic flow problems involving complex geometries. In the code, a non-staggered grid arrangement is used and the governing equations in a generalized curvilinear co-ordinate system are solved following the finite volume method. A special interpolation procedure developed by Rhie and Chow [11] is used to prevent pressure oscillations due to non-staggered grid arrangement. Pressure and velocity coupling is achieved through the SIMPLE algorithm [12]. The calculation results were declared converged when the maximum normalized residue of all the dependent variables was less than a prescribed convergence criterion, typically a value of 0.005 per cent for two-dimensional problems and 0.5 per cent from three-dimensional problems.

3. FLOW PROBLEMS AND SIMULATED RESULTS

3.1. Pure convection of a box-shaped step profile in an oblique velocity field

The flow configuration shown in Figure 3 constitutes a test problem for examining the performance of a numerical approximation to convection because of the extremely sharp gradient in the scalar. This is a linear problem in which the velocity field is prescribed. The calculations are performed with a uniform mesh 59×59.

A comparison of the numerical solutions obtained with the UPWIND, QUICK, and present WACEB schemes is presented in Figure 4. It can be seen that the UPWIND scheme results in a very diffusive profile for the scalar and the QUICK scheme produce overshoots and undershoots. It is noticed that the WACEB predicts a fairly good steep gradient without introducing overshoots or undershoots.

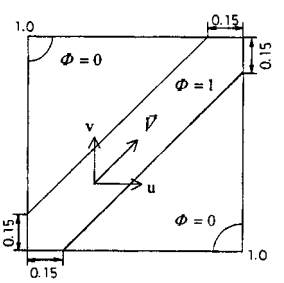

Figure 3. Pure convection of a box-shaped step.

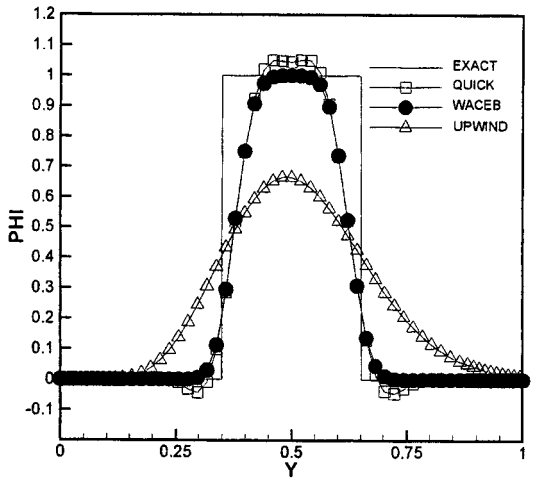

Figure 4. Scalar profiles along the centerline.

Figure 5 shows the computed scalar profiles with the different TVD slopes. A uniform mesh 119×119 is used. The larger slopes, such as 3.5 and 4, predict no significantly improved results as compared with the standard TVD slope of 2. However, when the slope is 4.5, overshoots are produced (see enlarged part of Figure 5). Therefore, in the following section, a slope of 2 is used.

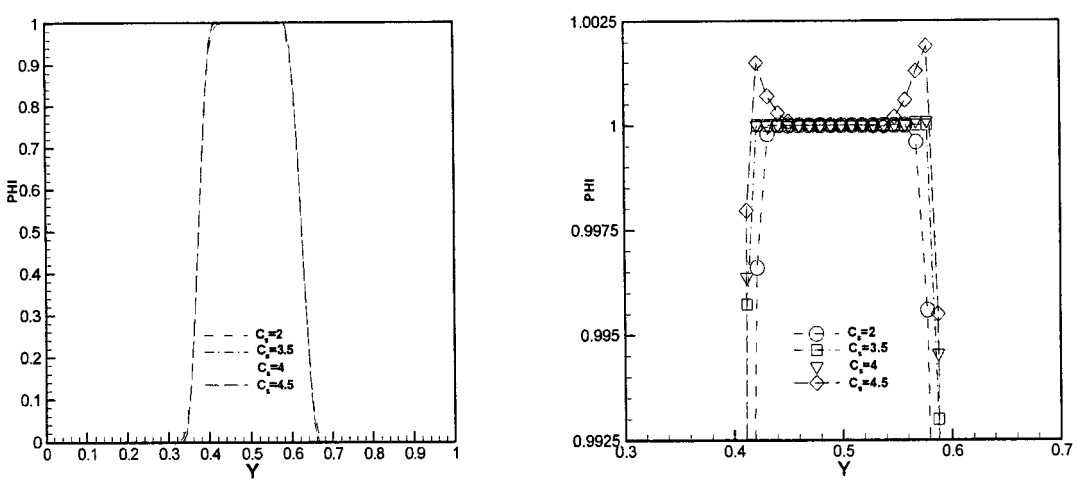

Figure 5. Predicted step profiles with different TVD slopes (119×119).

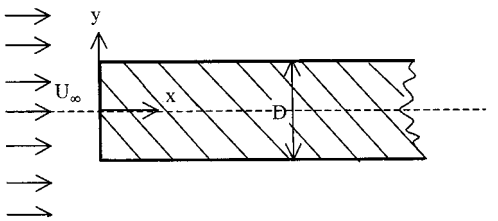

Figure 6. Flow over a blunt plate.

3.2. Two-dimensional turbulent flow around a blunt plate

Firstly, the two-dimensional turbulent flow around a blunt plate inside a wind tunnel, as depicted in Figure 6, is solved as an example of recirculating turbulent flows. Attention is focused here on the performance of the numerical schemes in predicting this complex recirculating turbulent flow. The inlet and outlet of the computational domain are located $12D$ upstream of separation and $15D$ downstream of reattachment respectively. The wind tunnel height is 20 times the plate thickness. Because of the symmetry of flow configuration, only one half of the flow region is chosen as the computational domain. Calculations are performed for a Reynolds number of 25000 based on the plate thickness D and inlet velocity.

At the inlet, uniform profiles are provided for velocities, turbulence kinetic energy, and specific dissipation rate. The turbulence kinetic energy and specific dissipation rate at the inlet are given as

$$k_{\text{in}} = 0.005 \cdot U_{\text{in}}^2, \qquad \omega_{\text{in}} = \frac{k_{\text{in}}}{1000 \cdot \nu}$$

At the outlet, a zero-gradient condition is applied for velocities and turbulent quantities. At the wall boundary, both velocities and turbulence kinetic energy are set to zero, and the specific dissipation rate is given according to the following equation:

$$\omega = \frac{2\nu}{\beta^* y^2} \quad \text{for } y^+ \leq 2.5$$

where y is the normal distance from the wall.

A non-uniform grid of 150×97 is employed, with the mesh refined in the near-wall region, shown in Figure 7. Table III gives the reattachment length using different grid systems. It shows that 150×97 grid distribution yields grid-independent results.

Figure 8 shows the predictions of streamwise velocity profiles with two different mixed procedures of numerical schemes. Also included in the figure are the experimental data of Djilali *et al.* [13]. It is seen that Method 1 and Method 2 produce somewhat different

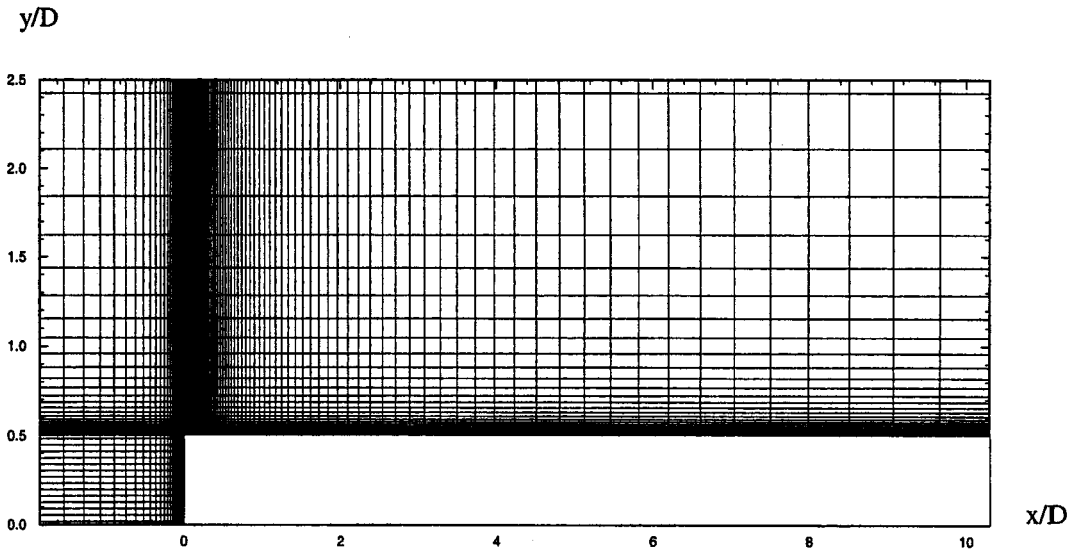

Figure 7. Typical grid layout around the blunt plate.

Table III. Reattachment length versus grid systems.

Grid systems	Experimental data	150×57	150×97	150×147
Reattachment length (Method 1)	4.5	4.42	4.85	4.91
Reattachment length (Method 2)	4.5	4.73	5.20	5.31

velocity profiles, particularly in the region between $x/D = 2$ and $x/D = 5$. It is explained that very different turbulence viscosity profiles are predicted by the two methods and then they feed back to the mean momentum equations. Note from Figure 9 that the diffusive nature of Method 2. The predictions by both methods are in fairly good agreement with the experimental data in the recirculating flow region. It is noteworthy that Method 1 improves approximately 10–20 per cent over Method 2. However, the predictions produce a slower velocity recovery downstream from the reattachment point. This appears to be a common feature of many reattaching flow calculations [14].

We also observe that in the separation region, a substantial discrepancy between the predictions by Method 1 and Method 2 occurs. From Table III, it can be seen that the predicted reattachment length with Method 2 is larger than that with Method 1. The UPWIND scheme produces a large numerical diffusion and tries to flatten and distribution of turbulence quantities, which leads to a lessening of turbulence energy as fluids flowing into a recirculating region and an enlargement of the separation region.

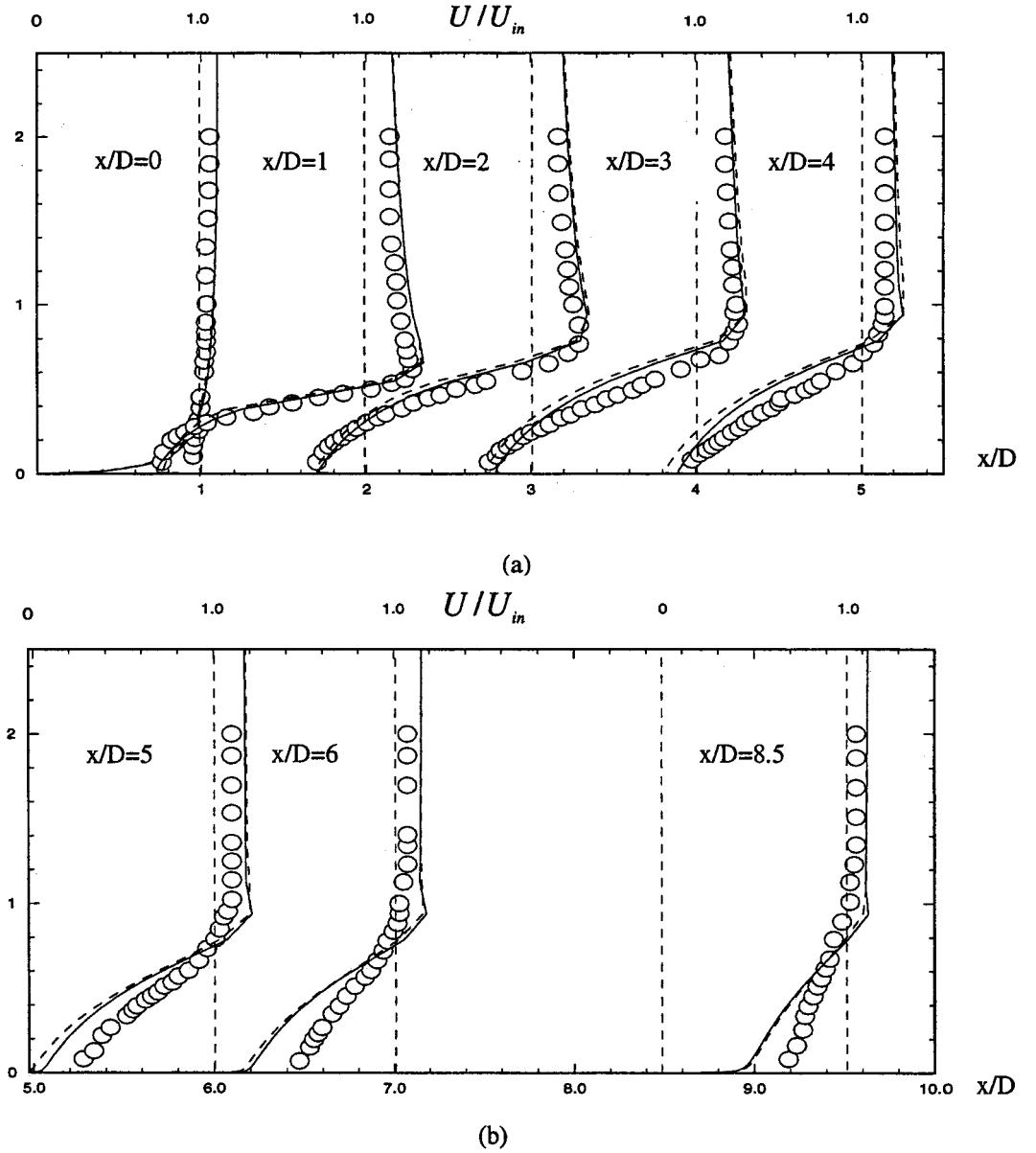

Figure 8. (a) and (b) Comparison of predicted and measured velocity profile. ○, Experimental data; —, Method 1; – – –, Method 2.

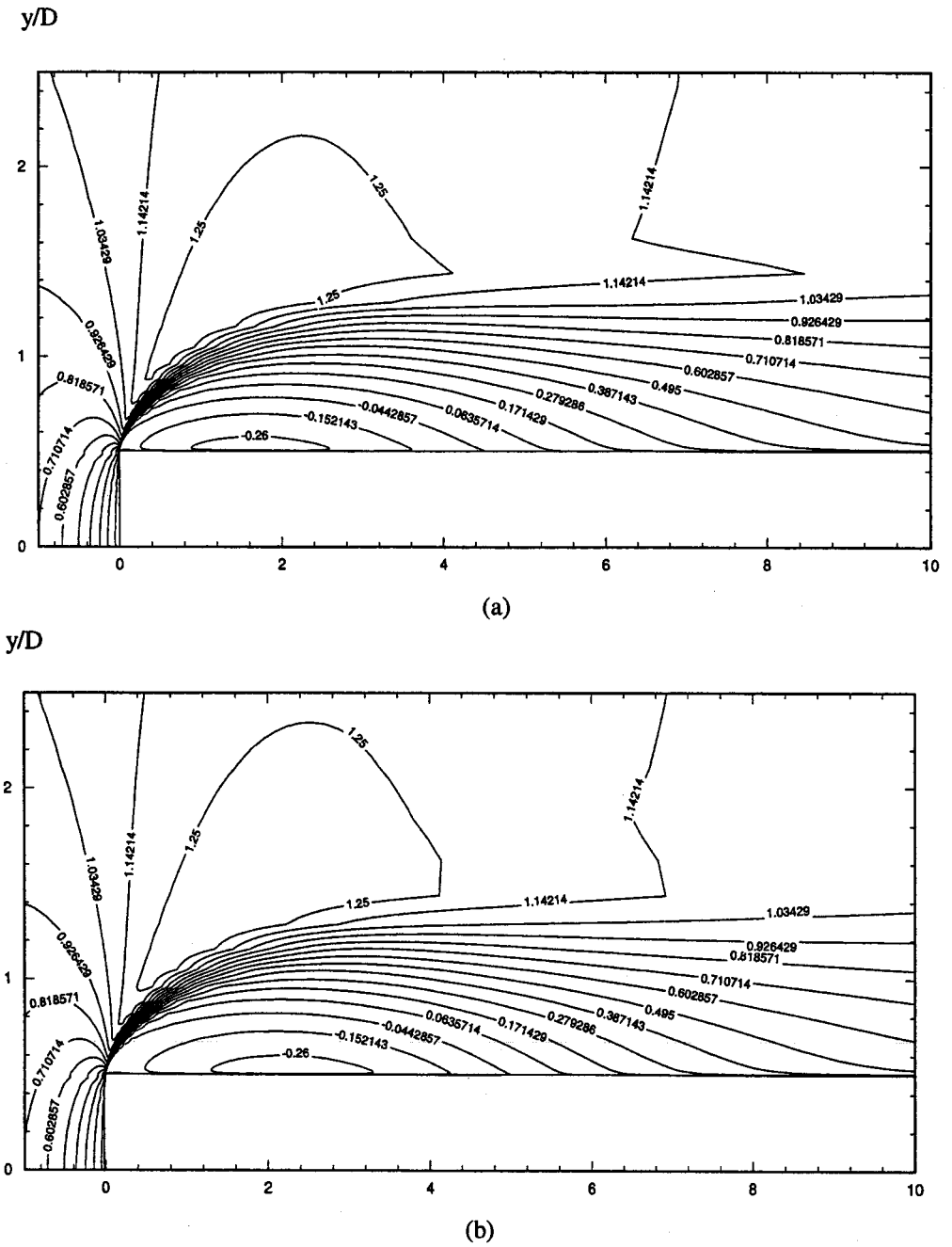

Figure 9. Mainstream velocity contour around the blunt plate predicted by (a) Method 1, (b) Method 2.

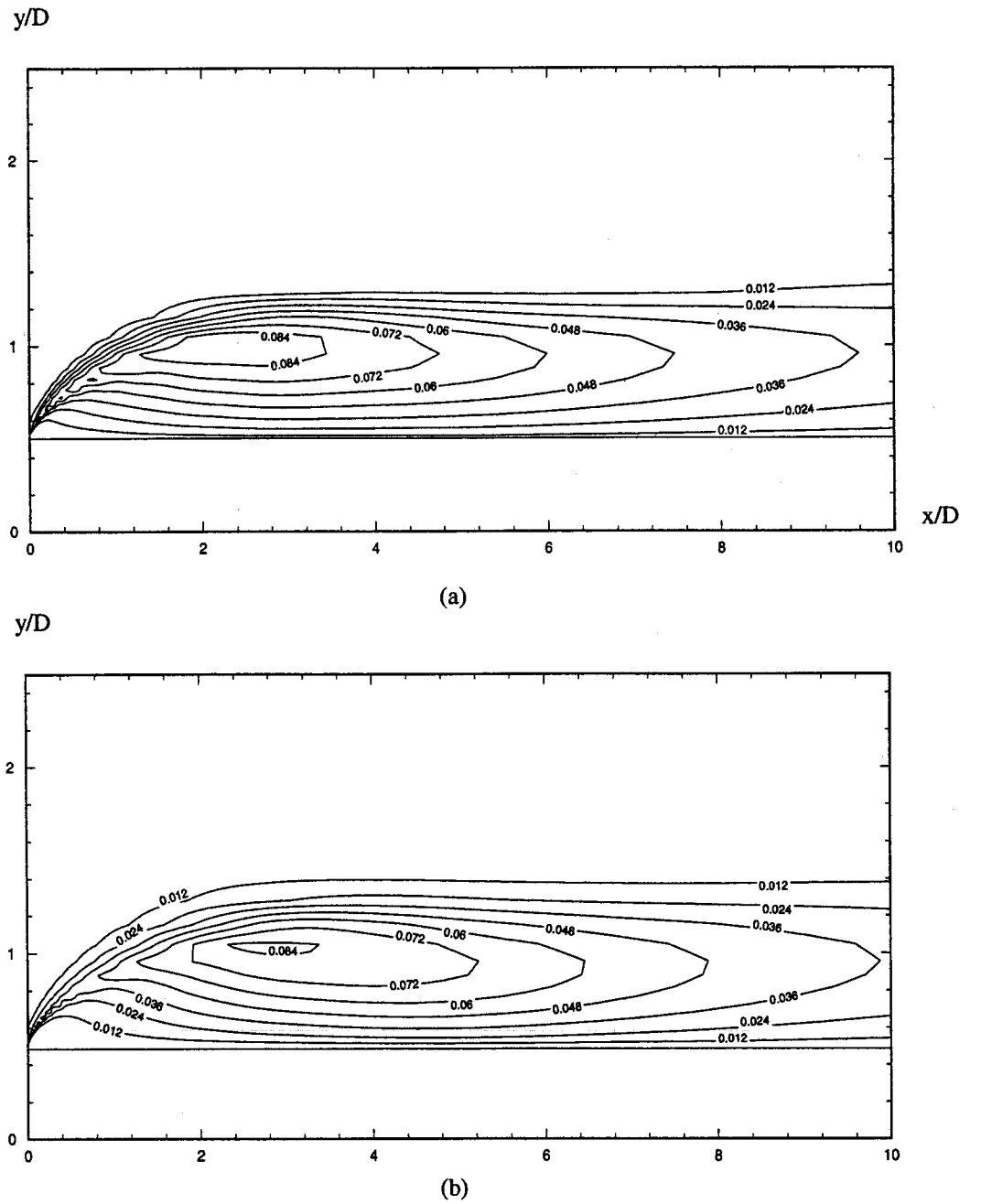

Figure 10. Turbulence kinetic energy (k/U_{in}^2) contour around the blunt plate predicted by (a) Method 1 (b) Method 2.

Figure 9 illustrates the velocity contours. It is noticed that the different velocity profiles with two methods mainly occur in the separation region and near the attachment point. Also, it is seen that the predicted reattachment length with Method 2 is larger than that with Method 1. The UPWIND scheme produces a large numerical diffusion and tends to flatten the distribution of turbulence quantities, which leads to a lessening of turbulence energy as the flow moves into a recirculating region and causes and enlargement of the separation region.

Figure 10 shows the turbulence kinetic energy contours predicted by two methods. The two methods present very different distributions. Near the zero streamline, the turbulence kinetic energy computed by Method 2 is lower than that of Method 1. This verifies the above conclusion. Therefore, it is concluded that for the recirculating flow, the mixed procedure of QUICK and UPWIND (Method 2) will produce substantially different velocity and kinetic energy profiles compared with the predictions of the mixed procedure of QUICK and WACEB (Method 1). It is recommended that for such flows, Method 1 should be employed.

3.3. Three-dimensional turbulent flow inside a moderately curved U-bend

The turbulent flow through a square-sectioned U-bend with moderate curvature $R_c/D = 3.35$, shown schematically in Figure 11, is numerically simulated in the present study as an example of three-dimensional turbulent flows. This type of flow involves a strong secondary motion and a very complex streamwise flow distribution, with a trough in velocity near the inside of the U-bend. A detailed numerical study has been reported in the literature by employing the algebraic stress model (ASM) closure [15]. The experimental study was carried out by Chang *et al.* [16]. The bulk Reynolds number, based on the hydraulic diameter and bulk velocity, is equal to 56700. Only the flow in the top half of the duct is computed because of the symmetry of the flow configuration. The inlet conditions are

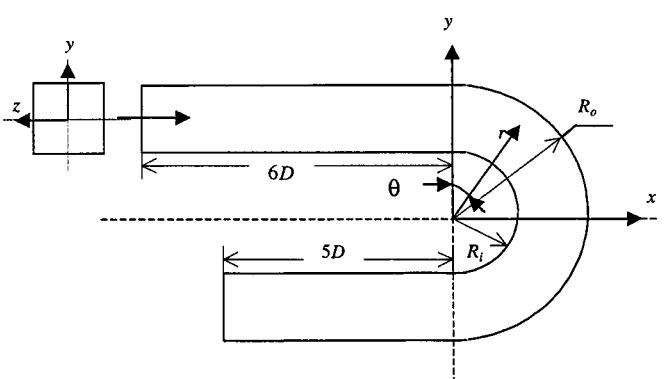

Figure 11. The square-sectioned U-bend of Chang *et al.* [16].

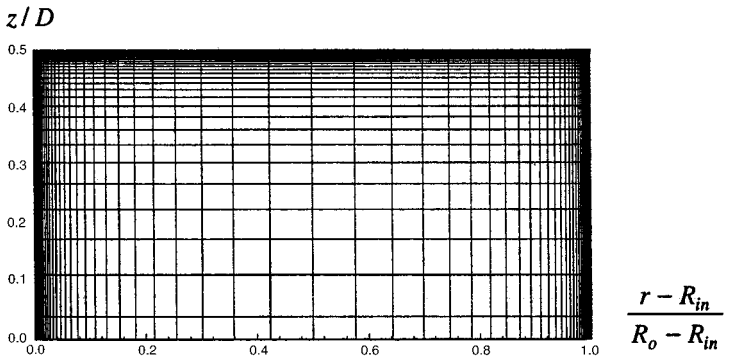

Figure 12. Grid layout of cross-section in the U-bend.

generated from a separate computation of a fully developed turbulent flow in a straight duct that has the same mean flow Reynolds number as in the experiment. At the exit of the computational domain, a zero-gradient condition is applied for velocities and turbulent quantities.

On the cross-sectional plane, a non-uniform grid of 89×45 is employed, with the mesh refined in the near-wall region, as shown in Figure 12. In the streamwise direction, uniform meshes are used with four planes per diameter. The present study shows that grid-independent results can be achieved with the mesh $110 \times 89 \times 45$.

The selected numerical results are shown in Figure 13 for the mainstream velocities, and in Figure 14 for the radial velocities. It is noticed that the computed results with Method 1 and Method 2 are practically indistinguishable. Also, the experimental data [16] are included in the figures. It is seen that the turbulence model adopted here has faithfully predicted the measured mean flow features through the U-bend. For example, at $\theta = 90°$ and $\theta = 130°$, the streamwise velocity profiles on the symmetrical plane in the trough are well captured. We also note that a substantial discrepancy exists somewhere between predictions and measurements. In the literature [15], similar results were obtained by using the ASM. It can be explained that the turbulence model adopted here needs further modification to represent the curvature effects. The mainstream velocity contours predicted by two procedures, illustrated in Figure 15, also verify this conclusion.

The contours of the turbulence kinetic energy predicted are shown in Figure 16. It is seen that a substantial difference appears. It illustrates that the UPWIND scheme introduces serious numerical diffusion to turbulence equations, which flattens the distributions of turbulence quantities. Interestingly, these different turbulence kinetic energy profiles do not seem to influence the mean velocity distributions.

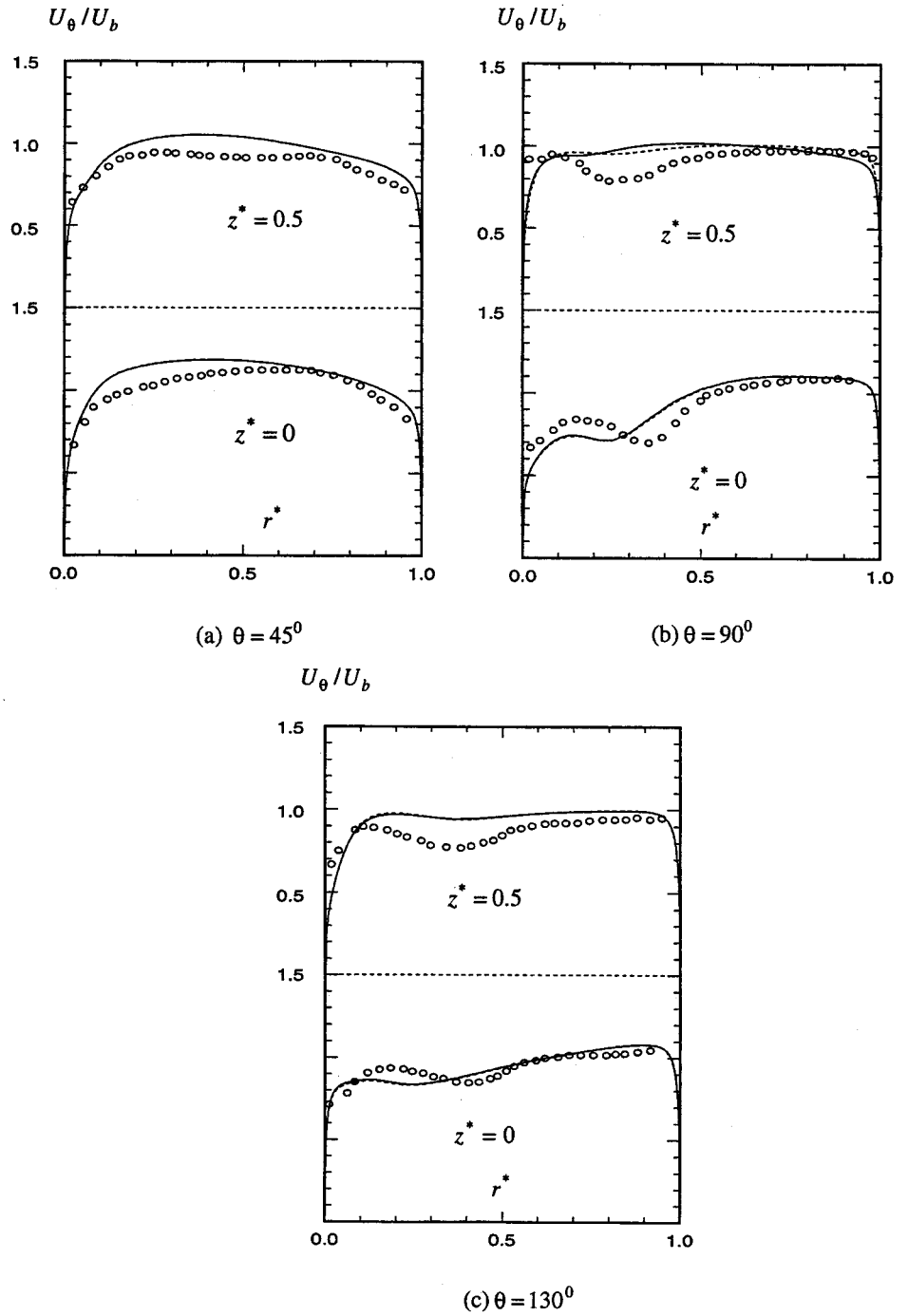

Figure 13. Streamwise velocity profile in the U-bend (○, experimental data [16]).

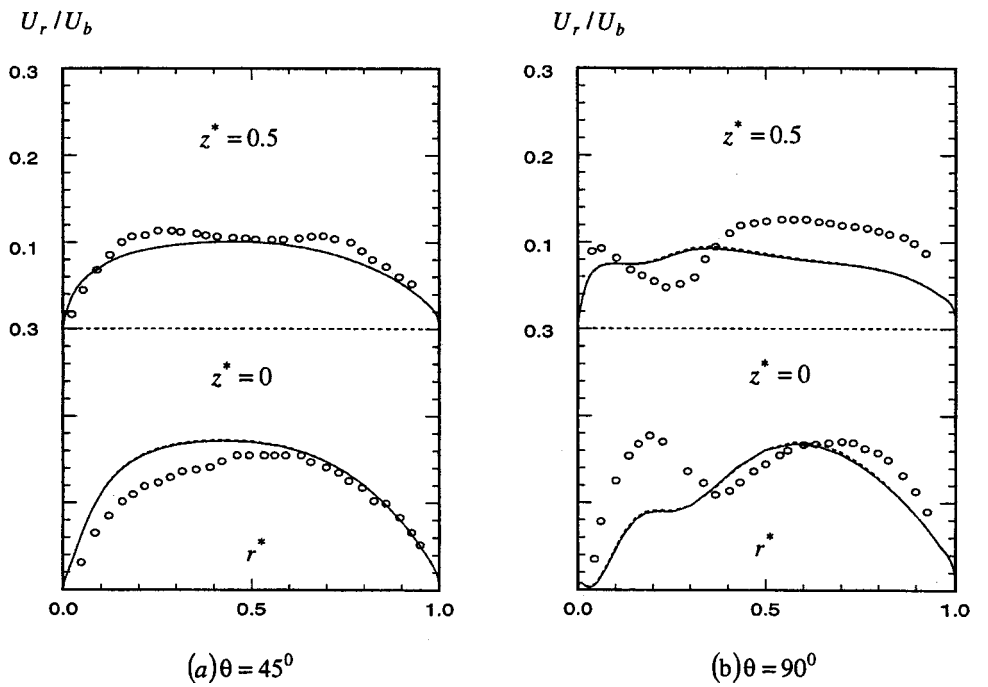

Figure 14. Radial velocity profile in the U-bend (○, experimental data [16]; —, Method 1; – – –, Method 2).

4. CONCLUSIONS

In this study, the WACEB scheme is extended to simulate two-dimensional separated flow around a blunt plate and three-dimensional turbulence flow inside a moderately curved U-bend. The following conclusions emerge through this study:

1. The WACEB scheme is very easy to implement in a general computer program and it does not need any under-relaxation treatment for the weighted average coefficient calculation.
2. The WACEB scheme retains the ability of QUICK to reduce numerical diffusion with the addition of the feature of not introducing overshoots or undershoots.
3. The numerical study shows that the slopes have a range from 2 to 4. Over this range, the numerical prediction will exhibit either diffusive results or overshoot results.
4. For the turbulent recirculating flow, a substantial difference in both velocities and turbulence kinetic energy is produced with two different mixed procedures. Method 2 predicts a longer separation region than Method 1. Compared with the experimental data, Method 1 can produce better results than Method 2.
5. For the moderately curved turbulent flow, although the predictions of velocity distributions with the two mixed procedures are very similar, a noticeable difference in turbulence kinetic energy appears.

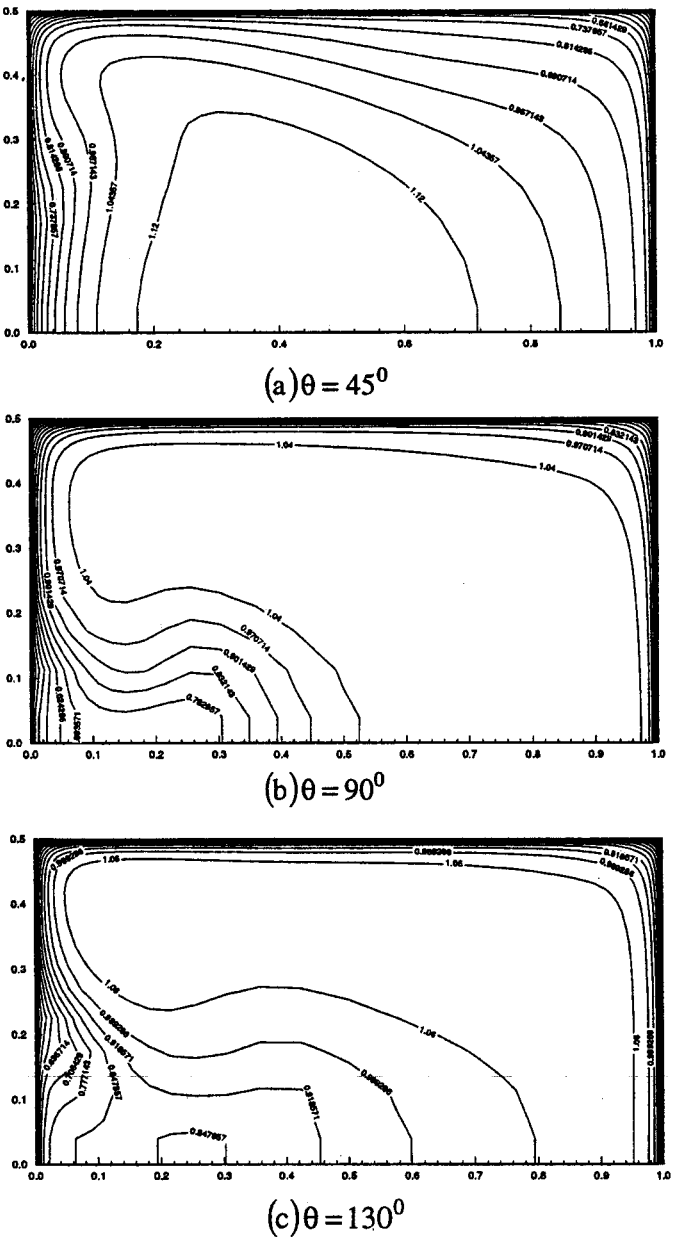

Figure 15. Streamwise velocity contours predicted by (a) Method 1; (b) Method 2.

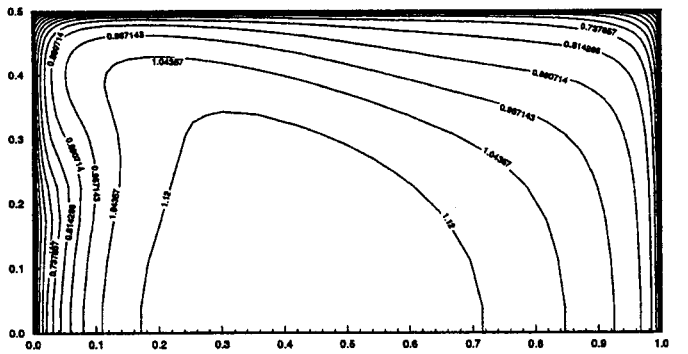

(a) $\theta = 45^0$

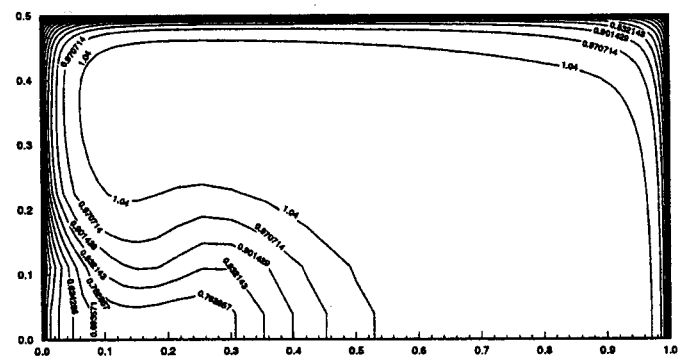

(b) $\theta = 90^0$

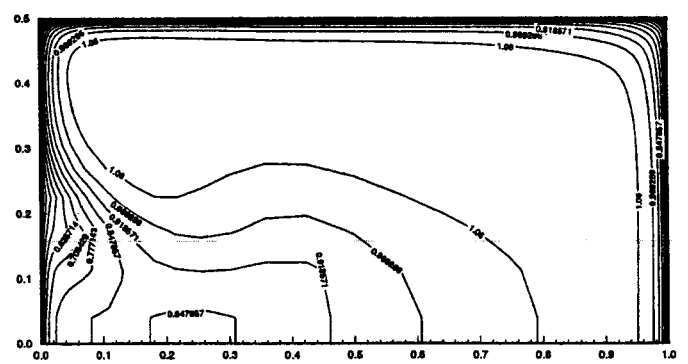

(c) $\theta = 130^0$

Figure 15 (*Continued*)

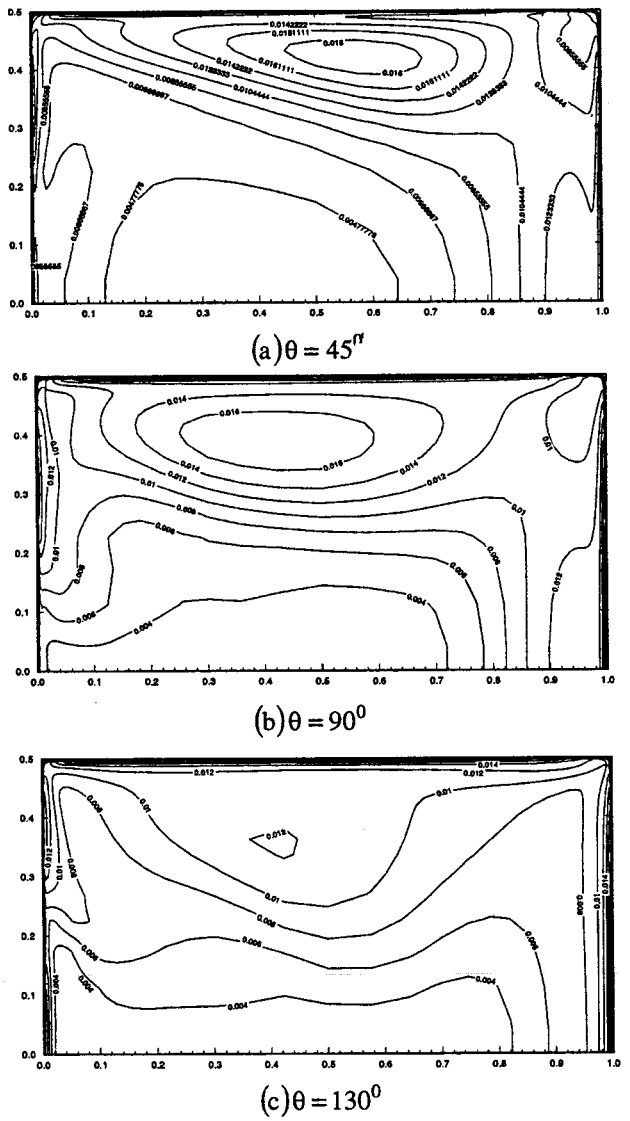

Figure 16. Turbulence kinetic energy contours predicted by (a) Method 1, (b) Method 2.

6. A discrepancy exists between numerical simulations and experimental data. The reason is the limit of the linear two-equation turbulence model to such complex turbulent flows with extra strain rates. Therefore, in order to obtain reliable predictions of turbulent fields, both bonded higher-order convection schemes and refined turbulence models have to be used.

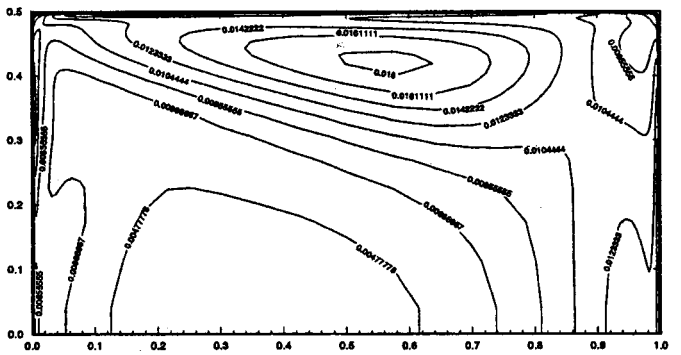

(a) $\theta = 45^0$

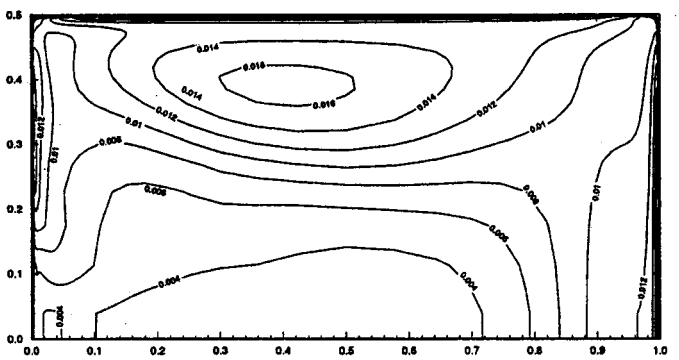

(b) $\theta = 90^0$

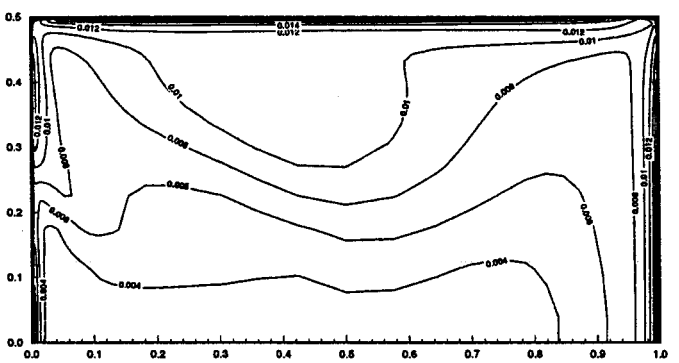

(c) $\theta = 130^0$

Figure 16 (*Continued*)

APPENDIX A. NOMENCLATURE

a, b, c	weighted average coefficients
D	thickness of plate

k	turbulence kinetic energy
P	mean pressure
r	radial distance
R_c	$\equiv (R_i + R_o)/2$
Re	Reynolds number ($= U_b D/\nu$)
Re_T	turbulence Reynolds number($= \kappa/(\omega\nu)$)
R_i, R_o	inner and outer radius for curved channel
U_b	bulk velocity
u, v, w	Cartesian velocities
x, y, z	Cartesian co-ordinates

Greek letters

ν, ν_t	laminar viscosity
ω	specific dissipation rate
Φ	arbitrary transport variables

Subscripts

ξ, η, ζ	derivatives

REFERENCES

1. Price HS, Varga RS, Warren JE. Application of oscillation matrices to diffusion–convection equations. *Journal of Mathematics in Physics* 1966; **45**: 301–311.
2. Leonard BP. A stable and accurate convective modelling procedure based on quadratic upstream interpolation. *Computer Methods in Applied Mechanics and Engineering* 1979; **19**: 59–98.
3. Song B, Liu GR, Lam KY, Amano RS. Four-point interpolation schemes for convective fluxes approximation. *Numerical Heat Transfer, Part B* 1999; **35**: 23–39.
4. Zhu J, Leschziner MA. A local oscillation-damping algorithm for higher-order convection schemes. *Computer Methods in Applied Mechanics and Engineering* 1988; **67**: 355–366.
5. Leonard BP. Simple high-accuracy resolution program for convective modelling of discontinuities. *International Journal for Numerical Method in Fluids* 1988; **8**: 1291–1318.
6. Gaskell PH, Lau AKC. Curvature-compensated convective transport: SMART, a new boundedness preserving transport algorithm. *International Journal for Numerical Methods in Fluids* 1988; **8**: 617–641.
7. Zhu J. On the higher-order bounded discretization schemes for finite volume computations of incompressible flows. *Computer Methods in Applied Mechanics and Engineering* 1992; **98**: 345–360.
8. Song B, Liu GR, Lam KY, Amano RS. On a higher-order bounded discretization scheme. *International Journal for Numerical Methods in Fluids* 2000; **32**: 881–897.
9. Wilcox DC. *Turbulence Modeling for CFD* (1st edn). DCW Publishers: Los Angeles, 1993.
10. Khosla PK, Rubin SG. A diagonally dominant second-order accurate implicit scheme. *Computers and Fluids* 1974; **2**: 207–209.
11. Rhie CM, Chow WL. A numerical study of the turbulent flow past an isolated airfoil with trailing edge separation. *AIAA Journal* 1983; **21**: 1525–1532.
12. Patankar SV. *Numerical Heat Transfer and Fluid Flow*. McGraw-Hill: New York, 1980.
13. Djilali D, Gartshore I, Salcudean M. Calculation of convective heat transfer in recirculating turbulent flow using various near-wall turbulence models. *Numerical Heat Transfer, Part A* 1989; **16**: 189–212.
14. Nallasamy M. Turbulence models and their application to the prediction of internal flows: a review. *Computers and Fluids* 1987; **15**: 151–194.
15. Li HY. Numerical studies for turbulent flows inside U-bends. PhD thesis, University of Manchester Institute of Science & Technology, 1995.
16. Chang SM, Humphrey JAC, Modavi A. Turbulent flow in a strongly curved U-bend and downstream tangent of square cross-section. *Phsyco-Chemical Hydrodynamics* 1983; **4**: 243–251.

